Theor. Comput. Fluid Dyn. (2022) 36:943–967
https://doi.org/10.1007/s00162-022-00632-z

ORIGINAL ARTICLE

B. Shruti · Md. Mahbub Alam · A. Parkash · S. Dhinakaran

LBM study of natural convection heat transfer from a porous cylinder in an enclosure

Received: 28 May 2022 / Accepted: 3 October 2022 / Published online: 28 October 2022

Abstract Natural convection heat transfer from a porous cylinder put at various positions in a square, cooled enclosure, with air as the working fluid, is investigated in this work. The following setups are taken into account: The hot cylinder is placed in the middle of the enclosure, near the bottom, top, right sides, along diagonal as top-diagonal and bottom-diagonal. The cylinder and the enclosure walls are kept hot and cold, respectively. The lattice Boltzmann method is used to perform a numerical analysis for Rayleigh number $10^4 \leq Ra \leq 10^6$ and Darcy number $10^{-6} \leq Da \leq 10^{-2}$. The results are plotted as streamlines, isotherms, and local and mean Nusselt number values. The amount of heat transported from the heated porous cylinder is determined by varying Ra, Da, and the cylinder location. Even at a lower Rayleigh number (10^4), the average Nusselt number grows by nearly 70 % as the cylinder moves from the centre to the bottom and 105% as it moves to bottom-diagonal location when $Da = 10^{-2}$. At $Ra = 10^6$ and $Da = 10^{-2}$, the heat transfer rate of the cylinder located near the corner of the enclosure at the bottom wall increases by approximately 33% when compared to the case of the cylinder in the centre. Convective effects are more noticeable when the cylinder is positioned towards the enclosure's bottom wall. This research is applicable to electronic cooling applications in which a collection of electronic components is arranged in a circular pattern inside a cabinet.

Keywords Porous cylinder · Enclosure · Darcy number · Natural convection · Lattice Boltzmann method

List of symbols

C_1, C_2	Binary constants
D	Diameter of cylinder (m)
c_{F}	Non-dimensional Forchheimer term
δ	Distance from centre (δx or δy in x and y direction)
c_s	Speed of sound (ms^{-1})
G	Body force due to gravity (N)

Communicated by Vassilios Theofilis.

B. Shruti · S. Dhinakaran (✉)
The Centre for Fluid Dynamics, Department of Mechanical Engineering, Indian Institute of Technology Indore, Simrol, Indore 453 552, India
E-mail: ssdhinakar@gmail.com; sdhina@iiti.ac.in

Md. M. Alam
Center for Turbulence Control, Harbin Institute of Technology (Shenzhen), Shenzhen 518055, China

A. Parkash
Department of Mathematics, Indian Institute of Technology Indore, Simrol, Indore 453 552, India

Da	Darcy number $\frac{K}{D^2}$
N	Number of lattices on the cylinder
d_p	Particle diameter (m)
Nu_{L}	Local Nusselt number $\frac{\partial\theta}{\partial n}$
e_i	Discrete lattice velocity in direction i, $\frac{\Delta x_i}{\Delta t}$
Nu	Nusselt number $\frac{hL}{K}$
F	Body force due to presence of the porous medium (N)
p	Dimensionless pressure $\frac{p*}{\rho u_\infty^2}$
F_i	Total force term due to porous medium (N)
Pr	Prandtl number $\frac{\nu}{\alpha}$
F_b	Boussinesq force term (N)
Ra	Rayleigh number $\frac{g\beta\Delta T L^3}{\alpha\nu}$
g	Gravitational acceleration (ms^{-2})
u	Non-dimensional x-component velocity (ms^{-1})
f_i	Particle distribution function along ith link direction
v	Non-dimensional y-component velocity (ms^{-1})
f_i^{eq}	Equilibrium distribution function along ith link direction
U	Actual velocity (ms^{-1})
V	Auxiliary velocity (ms^{-1})
g_i	Temperature distribution function along ith link direction
w_i	Weighing factor in direction i
g_i^{eq}	Equilibrium distribution function of temperature ith link direction
x,y	Non-dimensional horizontal and vertical coordinate
L	Length of enclosure (m)
x^*,y^*	Dimensional horizontal and vertical coordinate

Greek symbols

ρ	Fluid density (kg m^{-3})
ϵ	Porosity
τ	Dimensionless relaxation time for density
ν	Fluid kinematic viscosity ($\mathrm{m}^2\mathrm{s}^{-1}$)
τ'	Dimensionless relaxation time for temperature
μ	Fluid dynamic viscosity (N s m^{-2})
t	Non-dimensional time $\frac{t*u_\infty}{H}$
Λ	Viscosity ratio $\frac{\mu_e}{\mu}$
Δt	Time step (s)
α	Thermal diffusivity ($\mathrm{m}^2\mathrm{s}^{-1}$)
Δx	Lattice space
β	Thermal expansion coefficient $\frac{Ra\,\alpha\,\nu}{g\Delta T L^3}$ (K^{-1})
θ	Dimensionless temperature $\frac{T-T_\infty}{T_w-T_\infty}$
σ	Thermal conductivity ratio

Subscripts

avg	Average
w	Wall
∞	Far field value
e	Effective
o	Inlet value
f	Fluid
M	Mean value
l	Local value of variable
i	Lattice link direction

Superscripts

$*$ Dimensional form of variables

1 Introduction

Natural convection in an enclosure is a fascinating subject of study because of its numerous applications in the cooling electronic components, nuclear reactors, solar panels, building thermal design, and heat exchangers. Electronic components are the backbone of computers in today's technological age. Massive research efforts are underway because it has applications in almost every industry imaginable, including aerospace, biomedical, defence, research organisations, and enterprises. Microchips are also stacked in an optimised space due to the miniaturisation of electronic devices. These gadgets require appropriate cooling to function properly. External fans with modest forced convection and additional buoyant effects are prevalent. To reduce power consumption and increase heat dissipation, an appropriate cooling mechanism must be designed. The literature [1–5] contains numerous studies on flow and heat transfer from cylinders in the field of thermal engineering. These classic studies in fluid mechanics and heat transfer have theoretical and practical value.

Porous medium is widely known for its efficient cooling [1]. The goal of this research is to study the natural convection heat transfer from a hot porous cylinder in an enclosure. The analysis is carried out by changing the placement of the cylinder and measuring the change in heat transfer rate. Heat transfer from solid or porous bodies in an enclosure has been carried out by several researchers because of its practical significance. House et al. [2] analysed natural convection heat transfer in a differentially heated chamber containing a square cylinder. With air as the working fluid, the influence of dimensionless body size ($W/L = 0, 0.5, 0.9$), Rayleigh number (10^3–10^6), and thermal conductivity ratio of solid body and fluid (0.2 and 5) on heat transfer was investigated. Convective effects can be lessened by increasing the body's size (> 0.5) and the value of thermal conductivity ratios, according to their findings. The rate of heat transfer is reduced when the thermal conductivity ratio is higher for the same compact size. Alsabery et al. [3] investigated conjugate natural convection for Rayleigh numbers 10^2–10^6 with Al_2O_3–H_2O nanofluid using Buongiorno's two-phase model. The enclosure's corners were differentially heated, while the rest of the walls are adiabatic, and the heat-conducting solid square block is in the middle. The effect of thermal conductivity ratio (0.28, 0.76, 1.95, 7, and 16) and dimensionless solid block size (0.1–0.7) was investigated. The heat transfer performance of partially cooled and heated enclosures is stated to be influenced by the size of the solid block and the thermal conductivity ratio.

In addition, studies using circular cylinders in an enclosure have been discussed in the archival literature. Moukalled and Acharya [4] investigated natural convection heat transfer in a square enclosure with varied aspect ratios (D/L =0.1–0.3) and Rayleigh numbers (10^4–10^7) using a circular cylinder heated isothermally. It was discovered that for lower Rayleigh numbers (10^4), conduction effects dominate. Convection effects become more significant as the Rayleigh number increases, resulting in a quicker heat transfer rate. Using varying temperature boundary conditions, Roychowdhury et al. [5] carried out a natural convection analysis in an enclosure with an inner circular cylinder. Walls that are vertically insulated and heated with a cooled cylinder were also researched. The impacts of the Rayleigh number (10^4–10^6), Prandtl number (0.7 and 10), thermal boundary conditions, and aspect ratio (1.5, 2.5, 4, and 5) were investigated. The Nusselt number increases when $Pr = 10$. At aspect ratios of 4 and 5, thermal stratification was noticed as well. Nabavizadeh et al. [6] investigated the natural convection in an enclosure having a centrally placed sinusoidal cylinder. The amplitude and undulations on the cylinder surface are varied and different shapes are examined for Rayleigh number 10^3–10^6. The results report that increment in the number of undulations from 0.4 to 0.8 decreases the Nusselt number as fluid circulation hinders in space within gaps of cylindrical surface. On further increase of undulations beyond 8, Nusselt number enhances as the shape converts to a circle.

Using the lattice Boltzmann approach, Jami et al. [7] investigated laminar convection flow in a differentially heated cavity containing a heat-conducting cylinder for Rayleigh numbers 10^3–10^6 , $Pr = 0.71$ and temperature difference ratio (0, 10, 50). According to the research, the Nusselt number varies linearly with the temperature difference ratio for the same Rayleigh number. The average Nusselt number of hot walls drops as the temperature difference increases, whereas cold walls show the opposite pattern. In addition, Jami et al. [8] investigated the effect of cylinder position on convective heat transfer for $Ra = 10^3$–10^6 , $Pr = 0.71$ and temperature difference ratio (0 and 50). In the case of a cold cylinder (temperature difference ratio = 0), the maximum rate of heat transfer was seen near the centre location. When the heat-generating cylinder is moved from the left to the right and from the bottom to the top of the enclosure, the rate of heat dissipation on the hot wall decreases while the rate of heat dissipation on the cold wall increases.

Kim et al. [9] explored natural convection in a cold chamber containing a cylinder for Rayleigh numbers 10^3–10^6. The vertical position of the cylinder inside the enclosure is changed. The cylinder's position is reported to have a big influence on convection-induced heat transfer. The profile of total surface averaged Nusselt number of enclosure and cylinder for various vertical locations is symmetric for $Ra = 10^3$ and 10^4, with the lowest value when the cylinder is at the centre. The natural convection heat transfer from a uniformly heated (isoflux) circular cylinder inside a cavity was investigated by Hussain and Hussein [10]. The cylinder's vertical position was varied vertically (− 0.25 L to 0.25 L) and the Rayleigh number was altered between 10^3 and 10^6 in their experiment. Because the average Nusselt number fluctuates nonlinearly, the placement of the cylinder has a substantial impact on heat transport. When fluid flows near the enclosure's top and bottom walls, a thin boundary layer forms.

Yoon et al. [11] investigated natural convection heat transfer from a circular cylinder in a square enclosure at $Ra = 10^7$. The heated cylinder's position inside the cooled container is varied in the vertical direction. The flow pattern inside the enclosure varied with a change in the location of the heated cylinder, indicating the transition from a steady to unsteady regime. It was also discovered that when the cylinder position is between 0.05 and 0.18 units below the centre, the flow and heat transfer remain constant. In a similar study by Kang et al. [12], a heated cylinder dislocated along the horizontal and diagonal lines in the cavity was considered. The effect of arbitrary cylinder position on transitions from unsteady to steady and steady to unsteady was investigated. Thermal plumes, vortices, and a sequence of cells known as *Benard cells* were found to control flow unsteadiness at the enclosure's corners and centre. Along the horizontal line, the critical points were at a distance of 0.1L from the centre in the left and right directions. In the diagonal line, near the left upper corner, 0.05L and 0.16L were the lower and upper bounds for steady state. In the right lower quadrant, 0.2L and 0.09L were the lower and upper bounds. Beyond these distances, the flow and thermal fields were in a steady state.

Nithiarasu et al. [13] analysed a porous filled differentially heated cavity with constant or variable porosity (0.4–0.9) for Rayleigh number $10^3 - 5 \times 10^9$. The results show that thermal and flow field changes with porous layer thickness. Vijaybabu [14] conducted a numerical investigation of heat transfer from a porous circular cylinder inside a cavity filled with CuO–H_2O nanofluid. The effect of permeability and volume fraction of nanoparticles was analysed for Rayleigh numbers 10^3–10^6 and Darcy numbers 10^{-2} to 10^{-6}. The study revealed that the location of maximum entropy generation depends on permeability. The investigation of entropy generation and thermosolutal convection in a rectangular enclosure attached to a porous wall was conducted by Hu and Mei [15]. The parametric study analyses the effect of buoyancy ratio, Darcy number (10^{-9} to 10^{-1}), enclosure inclination ($0° - 90°$), porous wall thickness (0–1), and Soret and Dufour number (0–1.5). The authors predicted that increasing the Darcy number enhances the average Nusselt number by 90%, but in the case of the thicker permeable wall, the heat transfer performance declines up to 50%. At an inclination angle of 90°, minimum heat transfer rates are obtained.

The literature has extensive numerical research on natural convection heat transfer in a closed cavity and solid heated cylinders of various forms placed inside an enclosure. There has been no study of natural convection from a porous circular cylinder and the influence of its location inside a confined cooled enclosure to the authors' best knowledge. This research tries to close that gap. The goal is to investigate the impact of various parameters such as Rayleigh number, Darcy number, and cylinder placement on flow and heat transfer. It also allows for the optimal placement of a porous cylinder in an enclosure for maximum heat dissipation. The lattice Boltzmann method is used to simulate flow and heat transport around and through a porous circular cylinder in an enclosure in this numerical study. It is investigated how permeability and Rayleigh number affect flow and heat transfer. This research aids in the comprehension of flow dynamics and convective heat transfer in an enclosure. This study's representative application is the thermal management of heat exchangers and electronic components.

2 Mathematical formulation

2.1 Problem description and geometrical configuration

The flow and heat transfer from a heated porous circular cylinder inside a two-dimensional square enclosure of size L are investigated. The centre of the axis lies at the geometric centre of the enclosure. Figure 1 depicts the computational domain explored for this numerical analysis. The heated cylinder inside the enclosure is maintained at a constant temperature T_h. The temperature of the enclosure's walls is lower (T_C) than that of the cylinder. The cylinder is 0.4 L in diameter. Heat transfer from the cylinder is evaluated in five various

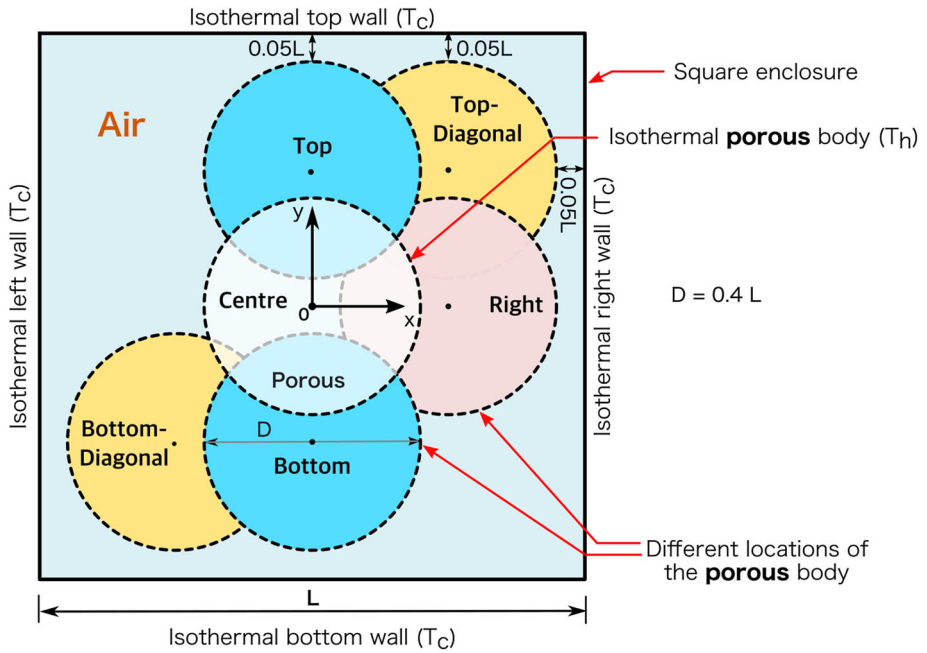

Fig. 1 Schematic diagram of the computational domain along with the imposed boundary conditions

configurations: Centre placement ($C_{\text{cyl}} = 0.5\,\text{L}, 0.5\,\text{L}$), top placement ($C_{\text{cyl}} = 0.5\,\text{L}, 0.75\,\text{L}$), bottom placement ($C_{\text{cyl}} = 0.5\,\text{L}, 0.25\,\text{L}$), right placement ($C_{\text{cyl}} = 0.75\,\text{L}, 0.5\,\text{L}$), top-diagonal ($C_{\text{cyl}} = 0.75\,\text{L}, 0.75\,\text{L}$), and bottom-diagonal ($C_{\text{cyl}} = 0.25\,\text{L}, 0.25\,\text{L}$). Here, C_{cyl} is the centre of the cylinder. The working fluid is presumably air ($Pr = 0.71$).

The following assumptions are made:

- Flow is two-dimensional, steady, laminar, and incompressible.
- Fluid is Newtonian and the fluid (air) properties are constant.
- Local thermal equilibrium is maintained between the porous cylinder and fluid flowing through and around it.
- The radiation effects of the cylinder are negligible.

2.2 Governing equations

The subsequent non-dimensional governing equations represent natural convection induced flow and heat transfer in a two-dimensional enclosure with a porous body [13].

$$\frac{\partial u}{\partial x} + \frac{\partial v}{\partial y} = 0 \tag{1}$$

$$\frac{1}{\epsilon}\frac{\partial u}{\partial \tau_t} + \frac{1}{\epsilon^2}\left(u\frac{\partial u}{\partial x} + v\frac{\partial u}{\partial y}\right) = -\frac{\partial p}{\partial x} + \frac{Pr}{\epsilon}\left(\frac{\partial^2 u}{\partial x^2} + \frac{\partial^2 u}{\partial y^2}\right) - C_1\frac{Pr}{Da}u - C_2\frac{1.75}{\sqrt{150}}\frac{1}{\sqrt{Da}} \times \frac{\sqrt{u^2+v^2}}{\epsilon^{3/2}}u \tag{2}$$

$$\frac{1}{\epsilon}\frac{\partial v}{\partial \tau_t} + \frac{1}{\epsilon^2}\left(u\frac{\partial v}{\partial x} + v\frac{\partial v}{\partial y}\right) = -\frac{\partial p}{\partial y} + \frac{Pr}{\epsilon}\left(\frac{\partial^2 v}{\partial x^2} + \frac{\partial^2 v}{\partial y^2}\right) - C_1\frac{Pr}{Da}v - C_2\frac{1.75}{\sqrt{150}}\frac{1}{\sqrt{Da}} \times \frac{\sqrt{u^2+v^2}}{\epsilon^{3/2}}v + Ra\,Pr\,\theta \tag{3}$$

$$\sigma\frac{\partial \theta}{\partial \tau} + \left(u\frac{\partial \theta}{\partial x} + v\frac{\partial \theta}{\partial y}\right) = \frac{k_{\text{eff}}}{k_f}\left(\frac{\partial^2 \theta}{\partial x^2} + \frac{\partial^2 \theta}{\partial y^2}\right) \tag{4}$$

Here, Prandtl number (Pr) is expressed as $Pr = \mu C_p/k_f$. C_1 and C_2 are the binary constants having value 0 for the fluid region and 1 in the porous region. k_f is the thermal conductivity of the fluid. Thermal properties of porous material (k_s) and fluid (k_f) are assumed identical, ($\sigma = 1, k_{\text{eff}} = k_f = k_s$) and the effective thermal conductivity is given as follows [16–18]:

$$k_{\text{eff}} = \epsilon k_f + (1 - \epsilon)k_s \tag{5}$$

The value of thermal conductivity ratio (σ) of solid porous material and fluid is considered to be unity for showing the flow effect of non-homogeneous variation in porosity [13]. The non-dimensional governing equations are attained with these characteristic scales as

$$x = \frac{x^*}{L}, y = \frac{y^*}{L}, t = \frac{t * u_\infty}{L}, p = \frac{p^* L^2}{\rho\alpha^2}, u = \frac{u^* L}{\alpha}, v = \frac{v^* L}{\alpha}, \theta = \frac{T - T_c}{T_h - T_c} \tag{6}$$

Here, the superscript * denotes the dimensional form of the variable.

2.3 Lattice Boltzmann method

The lattice Boltzmann method (LBM) is adopted for carrying out numerical simulations. LBM is a mesoscopic approach. In this method, the domain is discretized into lattices. Each lattice experiences collision and streaming. The governing parameters such as velocity, density and temperature are calculated with these steps. Values of velocity in the x and y direction, density, and temperature are calculated for all lattices across the domain. The convective terms in the LB equation are linear in contrast to the nonlinear terms in the Navier–Stokes equation.

The probability distribution function depends on the relaxation factor value, and macroscopic properties (such as density, velocity, and temperature) are mentioned in terms of LB units. So, all these values are mainly governed by kinematic viscosity (for fluid flow) and thermal diffusivity (for temperature). Hence, distribution function f and g will completely depend on these two parameters.

2.3.1 Lattice Boltzmann equation for velocity field

Collisions must occur between particles at each node before streaming can begin. The collision equation is given as follows [19]:

$$f_i\left(x + e_i\Delta t, t + \Delta t\right) - f_i(x, t) = -\frac{1}{\tau}\left[f_i(x, t) - f_i^{eq}(x, t)\right] + \Delta t F_b + \Delta t F_i \tag{7}$$

Here, f_i is the instantaneous particle distribution function, f_{eq} is corresponding equilibrium distribution function, e_i is velocity direction in vectors of particles in the lattice, F_i, force term for drag effects due to the presence of porous medium and $F_b$accounts for natural and forced convective effects. The D_2Q_9 model (Fig. 2) is used to simulate two-dimensional flow in this investigation. In this model, speeds of particles are expressed as [19]

$$e_i = \begin{cases} (0, 0), & i = 0 \\ (\cos[(i-1)\pi/2], \sin[(i-1)\pi/2])e, & i = 1 - 4 \\ (\cos[(2i-9)\pi/4], \sin[(2i-9)\pi/4])\sqrt{2e} & i = 5 - 8 \end{cases} \tag{8}$$

The BGK collision operator with single relaxation time (SRT) is denoted on the right side of Eq. (7). The particles relax towards equilibrium with a relaxation factor given by τ at each collision phase. The value of τ is the same for all particles in each lattice in the SRT model. The Chapman–Enskog equation links the LB fluid's viscosity to its dimensionless relaxation time. It is written as [19]

$$\mathbf{v} = \left(\tau - \frac{\mathbf{1}}{\mathbf{2}}\right)\Delta \mathbf{t}\,\mathbf{c_s^2} \tag{9}$$

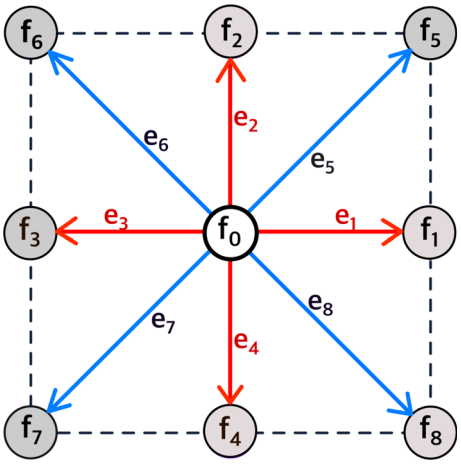

Fig. 2 Illustration of a lattice node for the D_2Q_9model for 2D problems [20]

In Eq. (7), a force term $F_i$is added, which explains the drag effects occurring due to the existence of a porous medium (porosity - ε) with a BGK collision factor. This force term is disabled by defining a value of 0 in the clear fluid region. The force term for the porous region is expressed as [19]

$$F_i = w_i \rho \left(1 - \frac{1}{2\tau}\right)\left[3(e_i \cdot F) + \frac{9}{\epsilon}(e_i \cdot U)(e_i \cdot F) - \frac{3}{\epsilon}(U \cdot F)\right]. \tag{10}$$

We have used D_2Q_9model in our study, hence $c_s = \frac{c_k}{\sqrt{3}}$. (c_s is the speed of sound and $c_k$are unit vectors along the lattice streaming directions) [19]. Here, F denotes the Darcy–Forchheimer force or the force of the body arising in porous region, which is considered to be both viscous and inertial forces and can be written as [19]

$$F = -\frac{\epsilon v}{K}U - \frac{\epsilon c_F}{\sqrt{K}}|U|\,U + \epsilon G. \tag{11}$$

In the above equation, v which denotes kinematic viscosity of the fluid, K is the permeability of the porous medium, $c_F = 1.75/\sqrt{150\epsilon^3}$, is the dimensionless Forchheimer term, $|U| = \sqrt{u^2 + v^2}$, where u and v are the components of velocity in the x and $y$directions, respectively, and G is the force of the body due to gravity. The updated equilibrium distribution function with terms of porosity is related as [19]

$$f_i^{eq} = w_i \rho \left[1 + 3(e_i \cdot U) + \frac{9}{2\epsilon}(e_i \cdot U)^2 - \frac{3}{2\epsilon}(U \cdot U)\right]. \tag{12}$$

Here, w_i denotes the weighting factor for each lattice link in the lattice arrangement. For the D_2Q_9 model, the value of weighting factors is $w_o = 4/9$, $w_o = 1/9$ for $i = 1, 2, 3, 4$ and $w_i = 1/36$ for $i = 5, 6, 7, 8$. After meso-level collision and streaming steps are performed with suitable boundary conditions, the macroscopic characteristics are calculated. The sum of the lattice distribution function of each point addresses the density of fluid at that point. Hence, the density (ρ) and velocity (U) of fluid can be determined through distribution function values as given below [19]

$$\rho = \sum_{i=0}^{8} f_i \tag{13}$$

$$\rho V = \sum_{i=1}^{8} e_i f_i + \frac{\Delta t}{2}\rho F. \tag{14}$$

Here, $V$is the auxiliary velocity due to the presence of the porous body. The actual velocity in this region can be evaluated with the following relation:

$$U = \frac{V}{c_0 + \sqrt{c_0^2 + c_1|V|}} \tag{15}$$

The two parameters $c_o$and c_1 in Eq. (14) are given by

$$c_0 = \frac{1}{2}\left(1 + \epsilon\frac{\Delta t}{2}\frac{v}{K}\right); \quad c_1 = \left(\epsilon\frac{\Delta t}{2}\frac{c_{\mathrm{F}}}{\sqrt{K}}\right) \tag{16}$$

Density variations are within the fluid. The fluid motion is driven by temperature or mass gradient, i.e. buoyancy force. Hence, there is an extra force term needed to be considered in solving the LB equation which is calculated by Boussinesq approximation. An additional force term $F_b$is added to the collision equation for natural convection. The calculation is done with Boussinesq approximation and is expressed as [19]

$$F_b = 3w_i g\beta\theta e_{iy} \tag{17}$$

Here, e_{iy}represents velocity vectors in the y-direction.

2.3.2 Lattice Boltzmann equation for temperature field

The lattice Boltzmann equation describing the temperature field is written as [19]

$$g_i\left(x + e_i\Delta t,\ t + \Delta t\right) - g_i\left(x, t\right) = -\frac{1}{\tau'}\left[g_i(x,t) - g_i^{eq}(x,t)\right]. \tag{18}$$

The Chapman–Enskog equation for calculation of thermal relaxation time is given as

$$\alpha = (\tau' - \frac{1}{2})\Delta t\, c_s^2. \tag{19}$$

The equilibrium distribution function g_{eq} can be expressed as

$$g_i^{eq} = w_i\theta\left[1 + 3(e_i \cdot U)\right]. \tag{20}$$

The fluid temperature θ is calculated from "g" distribution function as

$$\theta = \sum_{i=0}^{8} g_i. \tag{21}$$

2.4 Boundary conditions

No slip boundary condition and constant temperature boundary conditions ($\theta = 0$) are applied on the walls. These are expressed in terms of particle distribution functions. In terms of the lattice Boltzmann method, the boundary conditions used [19] are shown in Table 1. For the porous region, the porous force term in the flow field is applied according to Eq. (10). In the thermal field, a higher temperature ($\theta = 1$) is implemented in the entire porous region. We have defined a region for the porous circular body by the equation

$$\sqrt{(x - x_{\mathrm{cen}})^2 + (y - y_{cen})^2} \leq \text{radi}. \tag{22}$$

A dummy array is defined in the entire domain and its value is defined as "zero" in the clear fluid region and as "one" in the porous circular region. Further, we have imposed $\theta = 1$ in the entire domain of the porous region and not just at the surface. Also, $\theta = 0$ is implemented in the fluid region. Thermal boundary condition is defined by following equation

$$g_i = \theta * (w_i + \underline{w_i}) - \underline{g_i}. \tag{23}$$

Here, g_i represents distribution function for thermal field while $\underline{g_i}$denotes corresponding opposite link, w_i is the weighting factor for corresponding lattice link and $\underline{w_i}$ is the corresponding opposite link.

Table 1 Boundary condition used on the walls of the enclosure while employing LBM

Wall	Wall boundary conditions	Thermal boundary conditions
Left	$f_1 = f_3, f_5 = f_7, f_8 = f_6$	$g_1 = -g_3, g_5 = -g_7, g_8 = -g_6$
Right	$f_3 = f_1, f_7 = f_5, f_6 = f_8$	$g_3 = -g_1, g_7 = -g_5, g_6 = -g_8$
Top	$f_4 = f_2, f_8 = f_6, f_7 = f_5$	$g_4 = -g_2, g_8 = -g_6, g_7 = -g_5$
Bottom	$f_2 = f_4, f_6 = f_8, f_5 = f_7$	$g_2 = -g_4, g_6 = -g_8, g_5 = -g_7$

2.5 Dimensionless parameters

The dimensionless parameters used in this study are Rayleigh number and Darcy number. The Rayleigh number (Ra) is calculated on the basis of the number of lattices in characteristic height and is given by

$$Ra = \frac{g\beta\Delta T L^3}{\nu\alpha} \tag{24}$$

In this study, the length of enclosure L is considered as the characteristic height. Porous region is considered as the packed bed of spheres. The number of spheres, size, and space between them decides the amount of fluid flowing through the permeable region and indicates the porosity. The diameter of these spheres is denoted by d_p. The pressure drop of flowing fluid through a packed bed of spheres is evaluated through the Carman–Kozeny equation. The Darcy number (Da) represents the non-dimensional permeability of the porous body and is given as

$$Da = \frac{K}{D^2} = \frac{K}{N^2}. \tag{25}$$

Here, D is the characteristic height of a porous cylinder and K denotes permeability. Darcy number is also determined through the Carman–Kozeny relation [22–24] in terms of porosity (ϵ) as

$$Da = \frac{K}{D^2} = \frac{K}{N^2} = \frac{1}{180}\frac{\epsilon^3 d_p^2}{D^2(1-\epsilon)^2} \tag{26}$$

The equation calculates pressure drop of flowing fluid through a packed bed of spheres.

3 Numerical methodology

In this study, flow and heat transport are simulated using a FORTRAN code based on the lattice Boltzmann method. According to the equations stated in the preceding section, the flow and temperature boundary conditions are modified. The equation for collision is modified with additional force terms which account for natural convection. Buoyant force (F_b) is defined with Boussinesq approximation in the entire domain which comprises the acceleration due to gravity g. Its value depends on the Rayleigh number. In the domain, the initial velocity on all nodes is set to zero and the temperature on the heated region is set to 1. The stability of the solution depends on the value of $\sqrt{g\beta\Delta T L}$ which should be less than or equal to 0.1 [19]. The computations are terminated when the following convergence is achieved:

$$\frac{\sqrt{\sum_{ij}[u_{ij}^{n+1} - u_{ij}^{n}]^2}}{\sqrt{\sum_{ij}[u_{ij}^{n+1}]^2}} \le 1\times10^{-6}, \frac{\sqrt{\sum_{ij}[v_{ij}^{n+1} - v_{ij}^{n}]^2}}{\sqrt{\sum_{ij}[v_{ij}^{n+1}]^2}} \le 1\times10^{-6} \& \frac{\sqrt{\sum_{ij}[\theta_{ij}^{n+1} - \theta_{ij}^{n}]^2}}{\sqrt{\sum_{ij}[\theta_{ij}^{n+1}]^2}} \le 1\times10^{-6}. \tag{27}$$

Here, i and j denote locations of the nodes, n denotes the time step, $u(i, j)$ is the velocity in the x direction, v(i, j) is the velocity in the y direction, and $\theta(i, j)$ is the temperature.

Table 2 Comparison of the mean Nusselt number of the enclosure with literature [6] at $Pr = 0.7$

Ra	Present study	Nabavizadeh et al. [6]	Error (%)
10^3	1.57	1.63	3.68
10^4	1.60	1.65	3.03
10^5	2.45	2.43	0.82
10^6	4.46	4.48	0.44

The enclosure walls are cold, and the heated circular cylinder is centrally placed inside the cavity

Table 3 Comparison of the mean Nusselt number of the enclosure with literature [13] at $Pr = 1.0$

Da	Ra	Present study	Nithiarasu et al. [13]	Error (%)
10^{-2}	10^3	1.025	1.02	0.487
	10^4	1.693	1.69	0.177
	10^5	3.816	3.80	0.419
	5×10^5	6.180	6.20	0.322

In the study carried out by Nithiarasu et al. [13], the differentially heated cavity is filled with a porous medium having adiabatic top and bottom walls

3.1 Code validation

The present lattice Boltzmann code is validated by comparing the results for the Nusselt number in the case of natural convection heat transfer from a solid cylinder placed centrally in an enclosure. To consider the variation of different parameters, validation is done for the Rayleigh number, $Ra = 10^3 to 10^6$ and the cylinder diameter, $D = 0.4 \times L$. The obtained average Nusselt number on the wall accords with the values in the literature, as shown in Table 2. The numerical results obtained with the present LBM code show a good agreement with the results of the literature. Minimal deviation in results with the present code is due to the discretization method. The study by Nabavizadeh et al. [6] is based on the Lattice Boltzmann Method. The results of Nithiarasu et al. [13] are also validated for $Da = 10^{-4}$ and 10^{-2}. The satisfactory validation of the code provides confidence in the results obtained in the present study. The computed average Nusselt number compares well with the literature data as presented in Tables 2 and 3.

3.2 Grid dependence study

The computational domain is generated with a two-dimensional uniform mesh. Different grids are obtained for the various arrangements of circular cylinders considered in the study. The accuracy of results depends on grid size and characteristic height (L) of the enclosure. In LBM, the collision equation consists of a relaxation factor, which depends on the characteristic height. This factor plays an important role in the stability of a solution. Also, a higher grid size provides more stable and accurate results. The convergence rate of the solution decreases with an increase in the mesh size as the initial velocity decreases. Hence, an optimum size of the mesh is required for the study. The variation of the average Nusselt number on different mesh sizes is checked. Test simulations were done with 100×100, 200×200, 250×250 and 300×300 grid sizes. The size of each lattice is 1. The flow and heat transfer phenomenon near the porous region needs to be captured with utmost accuracy. Due to this fact, the characteristic height of the porous circular region is 0.4 times domain height *i.e.* $0.4 \times$ L. The grid independence study is done with the extreme parameters, $Da = 10^{-6}$ and $Da = 10^{-2}$ and intermediate value of Rayleigh number, 10^5 and the results are compared with a finer grid (300×300). It is observed that the results obtained beyond 250×250 mesh show less variation. The difference in the Nusselt number results between the coarse grid and the fine grid is less than 0.25%. It would generate results irrespective of the number of lattices in a grid. Considering the accuracy of results and computational time, 250×250 mesh size is found to be enough. Hence, 250×250 mesh is considered for further numerical simulations (see Table 4).

Table 4 Grid dependence analysis

Mesh size	$Da = 10^{-6}$		$Da = 10^{-2}$	
	Nu_M	% Difference	Nu_M	% Difference
100×100	2.3966	1.6832	4.1018	0.6746
200×200	2.4376	0.3413	4.1296	0.2429
250×250*	2.4460	0.1995	4.1397	0.2228
300×300	2.4509	–	4.1489	–

*Represents the mesh used in this study for further calculations

4 Results and discussion

A numerical analysis is carried out to investigate the flow and heat transport from a porous circular cylinder in an enclosure. The simulations are performed using the lattice Boltzmann method. The following parameters are used to investigate the impact of cylinder position on heat transport:

- Rayleigh Number $(Ra) = 10^4$, 10^5, and 10^6
- Darcy number $(Da) = 10^{-6}$, 10^{-4}, and 10^{-2}
- Porosity $(\epsilon) = 0.629$, 0.977, and 0.993 corresponding to $Da = 10^{-6}$, 10^{-4}, and 10^{-2}, respectively.

The diameter of the cylinder is 0.4 L. From the centre of the enclosure, the cylinder's position is varied horizontally, vertically and diagonally. Accordingly, the cylinder is moved to top, bottom, right, top-diagonal and bottom-diagonal. Since the flow and thermal characteristics are the same when the cylinder is placed on the left, top-left-diagonal and bottom-right-diagonal, these cases are not presented. The sections that follow take a closer look at the results.

4.1 Local Nusselt number

Nusselt number is a dimensionless parameter, defined as the ratio of convective to conductive heat transfer at the surface. It determines the effectiveness of thermal systems in heat dissipation. The local Nusselt number for each wall of the enclosure is calculated as

$$Nu_{\mathrm{L}} = -\frac{\partial T}{\partial n} \tag{28}$$

Figure 3 presents the local Nusselt number along the cold surface of the enclosure walls for different positions of the cylinder for $Ra = 10^4$–10^6. The distribution of local Nusselt numbers is symmetric about the top (A–B) and the bottom wall (C–D) of the enclosure. However, along with the right (B–C) and left (D–A) walls variations are asymmetric and alike for different vertical cylinder locations (i.e. top, centre, and bottom).

At $Ra = 10^4$ (Fig. 3a, b), the maximum value of the local Nusselt number is obtained at 0.25 L at mid (0.5 L) of the bottom wall when the cylinder is placed at bottom location. Another peak is obtained at 0.25 L of bottom and left wall when the cylinder is placed at bottom-diagonal position. These two locations of the cylinder have thinner boundary layer (see Fig. 8), in the region between the cylinder and bottom wall, which indicates more substantial convective effects. However, the minimum value close to zero is observed at all endpoints of walls. The variation along the right and left walls is analogous because of symmetrical thermal plumes along the vertical centreline of the enclosure. Moreover, with the increase in the Darcy number, a similar trend is observed and a minor increment in the magnitude of the maximum local Nusselt number is attained. The maximal value is obtained at $Da = 10^{-2}$ due to the enhancement in permeability.

When the cylinder is placed at the centre, the local maxima value is seen at the midpoint of the top wall (i.e. A–B). It occurs due to lower density hotter fluid flowing upwards. As it hits directly in the middle of the top wall which can be certified by Fig. 5a–c and 8a–c. The fluid density in the lower region of the enclosure is slightly higher, and hence, the intensity of heat transfer rate is lower near the bottom wall. The left and right walls show a similar trend, and its local maxima lies at a point slightly before its midpoint. The variation along the top wall and the bottom wall rises until reaches a maximum value in the midpoint of the wall and then falls to a value close to zero near endpoints. At $Da = 10^{-2}$, the distribution curve for the bottom wall (C–D) becomes more steep and the local maxima value decreases.

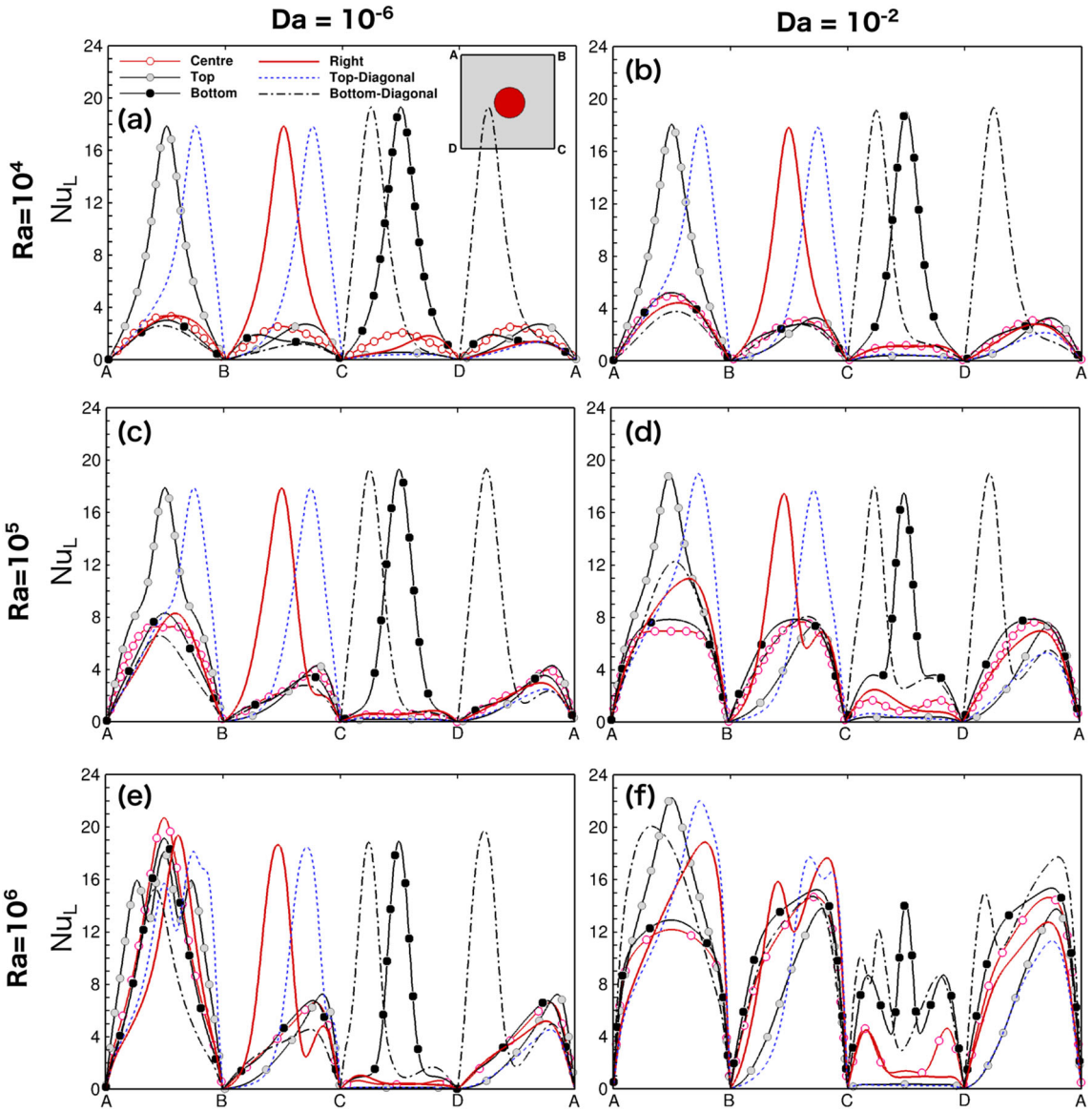

Fig. 3 Variation of local Nusselt number along the enclosure wall for different vertical locations of the cylinder at various Darcy numbers (10^{-6}, 10^{-4} and 10^{-2}) for **a**, **b** $Ra = 10^4$; **c**, **d** $Ra = 10^5$; **e**, **f** $Ra = 10^6$

As the cylinder is shifted towards the top wall, the distribution curve (Fig. 3a) rises significantly from point A to B. It attains local maxima at the wall's midpoint due to dense isotherms rising upwards in the region between the top wall and the cylinder. Along with the right (B–C) and left (D–A) wall, the value of the local Nusselt number increases continuously till the point after its midpoint. A slight shift in this point is noticed with an increase in Darcy number due to thermal plumes pointing towards the wall. A steep distribution curve exists along the bottom wall from C–D as the distance between wall and cylinder increases. Hence, it results in weak convective effects in a region close to this wall. As the Darcy number rises, the value of the local Nusselt number increases, depicting an elevated heat transfer rate.

Further, the position of the cylinder is changed closer to the bottom wall, the local Nusselt number increases and attains a peak value halfway through the bottom wall (C–D) due to dense thermal plumes near this point. The distribution of local Nusselt number along walls, A-B rises to its midpoint due to upwelling thermal plume at this point and then falls to the end. The variation on the right (B–C) and left (D–A) walls changes at $Da = 10^{-2}$ due to enhanced recirculation through the heated cylinder.

Further, the Rayleigh number is increased to 10^6, shown in Fig. 3e, f which presents the variation of the local Nusselt number along the enclosure wall. The general trend for the distribution of local Nusselt numbers at different Darcy numbers is not similar to the case of 10^4. The local Nusselt number value is also larger due to stronger convective effects. For $Ra = 10^6$ and $Da = 10^{-6}$, when the cylinder is at the centre (see Fig. 7a), the maximum local Nusselt number is achieved at the enclosure top wall (A–B) due to the presence of thermal plume pointing towards the midpoint of the top wall. On the right (B–C) and left (D–A) walls, the distribution curve increases to a point lying before the end of these walls and then falls suddenly to zero at its endpoint. Further, the curve becomes steep along the bottom wall (C–D) indicating negligible heat transfer to the wall, which can be certified in Fig. 10. At Darcy number 10^{-4}, the general trend is alike, but the magnitude of the distribution curve increases.

When the cylinder is shifted upwards, at $Da = 10^{-6}$, two undulations are found at the top wall (A–B) and a local maxima is observed at the midpoint. Flat distribution curve for the bottom wall (C–D) is observed, indicating negligible heat transfer to the bottom wall due to increment in the area between the cylinder and the bottom wall. For the right (B–C) and left (D–A) walls, the distribution rises until a point close to the wall ends and then falls suddenly. The magnitude of local distribution increases at $Da = 10^{-4}$ with a similar trend. With further increase in Darcy number to 10^{-2} (Fig. 3f), the shape of the local Nusselt number distribution curve changes to parabolic and its maximum value is attained at wall A–B. The presence of a thin thermal boundary layer leads to the peak value at the midpoint of the top wall.

When the cylinder is moved towards the bottom region of the enclosure for $Da = 10^{-6}$, the local maxima are seen at the middle of the bottom wall due to dense thermal plumes in the lower section of the cylinder near the bottom wall. At the top wall of the enclosure (A–B), the distribution curve increases until it attains a peak value, almost similar to the one obtained for the bottom wall (C–D) due to upwelling plumes. It can be stated that the rate of heat transfer in the middle of the top and bottom walls are almost equal in this case. The profile for the right (B–C) and left (D–A) walls is similar in all cases. The general trend is alike when $Da = 10^{-4}$ with increased magnitude. The maximum value is attained at mid of the top wall (A–B) due to the increased fluid velocity, and the second local maxima is achieved at mid of the bottom wall. At higher Darcy number 10^{-2}, the maximum value is achieved at right (B–C) and left walls (D–A) as the boundary layer is thinner near these walls, which was not observed in other cases. The value of the local Nusselt number at the top wall and bottom wall reduces in comparison with $Da = 10^{-4}$. As shown in Fig. 7g–i, the core of the inner eddy shifts downwards and more recirculation occurs. The isotherms in Fig. 10g–i are also parallel near these walls indicating a lower rate of heat transfer in the top and bottom walls.

The cylinder is also moved diagonally along the top-diagonal (see Fig. 5m–o) and bottom-diagonal location (see Fig. 5p–r). In top-diagonal position, local maxima is obtained at 0.75 L of top (A–B) and right (B–C) wall. The recirculation zone in the corner enhances heat transmission through these cold walls near the heated cylinder. As the Rayleigh number increases to 10^6, the number of undulations on the bottom-diagonal cylinder's profile increases. Also $Da = 10^{-2}$, two local maximas are obtained at 0.4 L of top wall and 0.8 L of left wall indicating the rise of thermal plumes towards top-left corner of enclosure, which lies directly above cylinder. Similarly, top-diagonal location has its local maxima at 0.8 L of top wall and 0.8 L of left wall as thermal plumes point towards left wall when convective effects are stronger.

4.2 Mean Nusselt number

The local Nusselt number (Nu_{L}) is calculated for each wall of the enclosure. The obtained $\mathrm{Nu_L}$ values of each wall (top, right, bottom, and left walls) are further integrated and then the mean is evaluated using the following equation:

$$Nu_{\mathrm{mean}} = \frac{1}{L}\int_0^L Nu_{\mathrm{L}}\,\mathrm{d}L \tag{29}$$

Here, the value of L is zero at the starting point on the wall and its value increases as we move further towards another end of the wall. (For example, as mentioned in Fig. 3a, A is the starting point and B is an endpoint of a top wall.) After solving the governing equations, the heat transfer rate is quantified with the mean Nusselt number in this study.

Figure 4 depicts the mean Nusselt number under the influence of Rayleigh number, Darcy number, and cylinder location. Remarkable impacts of Rayleigh number, Darcy number, and cylinder location can be

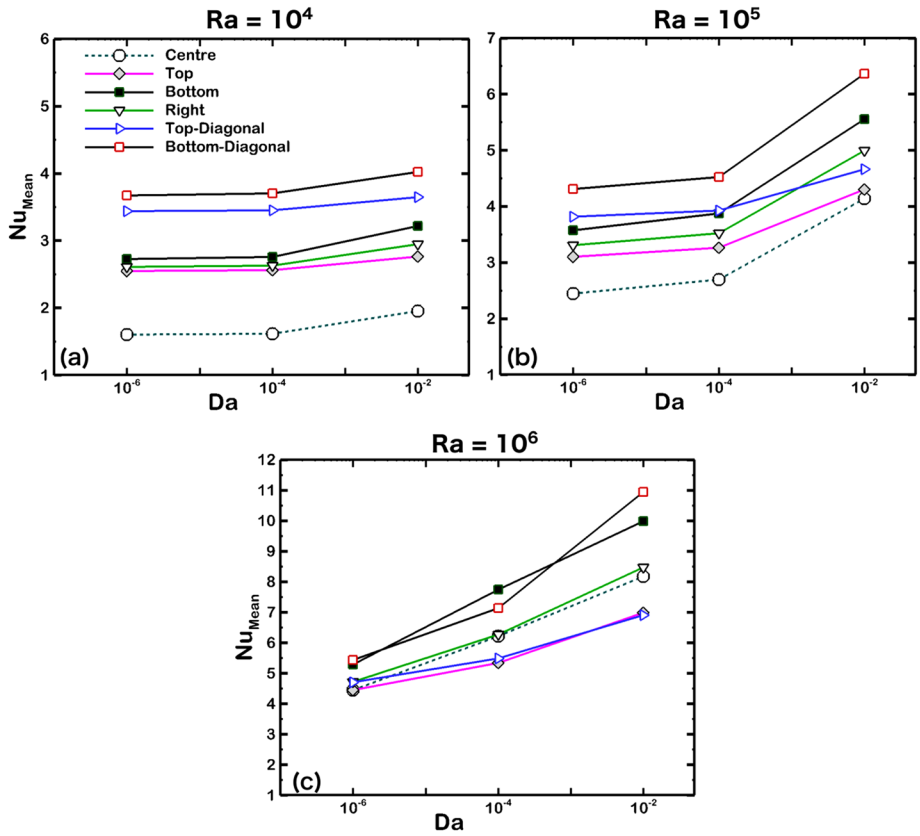

Fig. 4 Variation of mean Nusselt number (along enclosure wall for different locations of cylinder) with Darcy number for **a** $Ra = 10^4$, **b** $Ra = 10^5$, **c** $Ra = 10^6$

noticed. It is well known that an increment in Darcy and Rayleigh numbers increases the rate of heat transfer for all cylinder locations. The mean Nusselt number on the enclosure wall varies linearly with these parameters. The magnitude of Nu_{mean} increases as the Darcy number rises, owing to a stronger buoyant force that causes convective effects. The variation is also displayed with different positions of the cylinder inside the cavity. For all Rayleigh numbers, the value of Nu_{mean} is largest when the cylinder is placed at the bottom-diagonal position.

When the cylinder is placed at the bottom-diagonal, Nu_{mean} is at its greatest since the buoyant effects increase with the Rayleigh number. As a result, when marginal convection is reached at $Ra = 10^4$, the cylinder can be placed in bottom-diagonal or top-diagonal location for increased heat dissipation. The cylinder can also be placed towards the enclosure's bottom or right wall for a faster rate of heat transmission when natural convection effects are stronger. At a larger Rayleigh number, the rate of heat dissipation increases. At $Ra = 10^6$, the highest value of the mean Nusselt number is observed at the bottom position for an intermediate Darcy number (10^{-4}). Moreover, the mean Nusselt number for top-diagonal and top position is minimum in this case.

With the cylinder at bottom-diagonal position, the maximum Nu_{mean} value is attained. With variation in Darcy number, the rise in mean Nusselt number value is minimal at $Ra = 10^4$. When the Darcy number is increased from 10^{-6} to 10^{-4}, the rate of heat dissipation is negligible. However, at Rayleigh number 10^6, even at lower permeability levels, more liquid enters the permeable zone with greater velocity. For $Ra = 10^6$ and $Da = 10^{-2}$, there is a significant increase in the mean Nusselt number at the bottom-diagonal position of the cylinder.

4.3 Streamlines and isotherms

The streamline patterns and isothermal contours vary with the Rayleigh number and Darcy number. Air circulates inside the enclosure around and through the porous cylinder. The influence of the cylinder location on flow patterns is examined with streamline plots (see Figs. 5, 6 and 7). Thermal fields also significantly change with the variations in the parameters (Figs. 8, 9 and 10). The influence of the parameters can be observed through thermal plumes around the cylinder. The increment in the buoyant and permeability levels changes the density of temperature contours. Mixing heat with fluid depends on gravitational force also.

4.3.1 Effect of Rayleigh number

The buoyancy forces vary with the Rayleigh number. It is a well-known concept that at a lower Ra, the conduction effects are more dominant. The fluid circulates around the cylinder with a lower velocity. A small amount of fluid flows inside the porous cylinder due to stronger viscous resistance at $Ra = 10^4$ and $Da = 10^{-4}$. In the case of $Ra = 10^4$, convection effects can be observed for increased buoyant forces. As the Ra is increased further to 1×10^6, the velocity of fluid inside the enclosure increases. Fluid recirculates inside the enclosure after coming in contact with the heated cylinder. The temperature difference between the heated cylinder and enclosure wall induces heat flow towards the cold wall. The recirculation zone also moves towards the wall. It is found that at $Ra = 10^6$ fluid seeps inside the cylinder even at $Da = 10^{-4}$ which is not the case with lower Ra values. An enhanced rate of heat transfer is inferenced for all positions of the cylinder at $Da = 10^{-2}$ and $Ra = 10^6$ (Figs. 5, 6, 7, 8, 9, 10)

4.3.2 Effect of cylinder location

The porous cylinder placed at different locations inside the enclosure affects the flow and temperature field, which can be seen through Figs. 5, 6, 7, 8, 9 and 10 for Rayleigh number 10^4–10^6, while Da is varied from 10^{-6} to 10^{-2}. It can be observed that for all Ra and Da, flow and thermal fields are steady. A significant change in heat transfer is observed when the location of the cylinder is changed. When the cylinder is dislocated along the vertical centreline (*i.e.* top, centre and bottom), the hydrothermal characteristics are symmetrical.

Figure 5 depicts the flow field variation caused by a change in the placement of the cylinder inside the enclosure at $Ra = 10^4$. The Darcy number varies from $10^{-6}-10^{-2}$. For all positions, the fluid circulates around the cylinder at $Da = 10^{-6}$. For $Da = 10^{-6}$, two symmetric rotating eddies are visible when the cylinder is put in the centre (Fig. 5a–c). Each eddy has two inner vortices that are symmetric about horizontal and vertical axes. It's also worth noting that when $Da = 10^{-4}$, due to higher inertial resistance, just a little amount of fluid penetrates the porous cylinder. The inner whirls are no longer symmetric along the horizontal centre line in this scenario (see Fig. 5b). At $Da = 10^{-2}$, a single vortex is detected as the permeability increases with Darcy number, and the symmetry of both centrelines is restored. A large quantity of fluid enters the cylinder and comes into contact with the hot porous body. The fluid transports heat to the cold wall, accelerating heat dissipation. Figure 8a–c depicts the fluctuation in the thermal field. The isotherms for $Da = 10^{-6}$ and 10^{-4} are practically identical across the cylinder, indicating that the conduction mode is dominating with less heat transfer. At $Da = 10^{-2}$, contours get denser near the lower section of the cylinder as permeability increases, and heat transfer improves.

The single inner vortex moves downwards as the cylinder is pushed towards the top wall. Due to the increased space, the recirculation zone can be seen below the cylinder (see Fig. 5d–f). The eddy eye shifts towards the top wall as the Darcy number rises, allowing more fluid to enter the cylinder. Because the conductive rate of heat transfer is larger in the region between the top wall and the upper surface of the cylinder, the isothermal lines are denser. Thinner isotherms are detected below the cylinder as permeability increases, indicating improved heat transfer. The recirculation zone is in the upper part of the enclosure as the cylinder moves toward the bottom wall as seen in Fig. 5g–h. The streamline contour undergoes bifurcation in comparison with the centre and merges into a single inner whirl. With an increase in Darcy number, the eye of the single inner whirl shifts downwards, and an increased amount of fluid enters the cylinder. The thermal contours are denser in regions close to the bottom wall and lower portion of a cylinder, showing an increased conductive rate of heat transfer. At $Da = 10^{-2}$, thermal plumes point towards the top wall indicating the flow of lighter warmer fluid upwards due to density variation.

The porous cylinder is further shifted along a diagonal line of enclosure, towards top and bottom as shown in Fig. 5m–r. In the top-diagonal case, the clockwise recirculation zone is larger in the left region of the

enclosure (Fig. 5m–o). As the permeability level increases to $Da = 10^{-2}$, the eye of the innermost eddy shifts towards the vertical centreline. The small recirculating zone is observed in the top-right corner of the enclosure indicating accumulation of hotter fluid.

The bottom diagonal position of the cylinder is shown in Figs. 5p–r, 6p–r and 7p–r. The enlarged recirculation zone induces a higher convection rate towards the cold wall. As the Darcy number increases from $10^{-6}$to 10^{-2}, the shape of vortices over the cylinder transforms from rectangular to triangular. Small recirculating zone is also observed in the corner of the enclosure. The isotherms are denser near the corner of enclosure and coarser on the opposite side of the cylinder.

The symmetry of streamline and thermal fields around the vertical centreline distorts as the cylinder moves from the centre to the right, top-diagonal and bottom-diagonal location in the enclosure. In Fig. 5j–r, the giant vortex separates into two asymmetric smaller eddies above and below the cylinder.

The region of clockwise streamlines expands when the cylinder is pushed towards the right wall (Fig. 5j–l). A single compact inner vortex may be seen on the enclosure's left side, while two smaller asymmetric eddies form on the upper and lower right corners. At $Da = 10^{-2}$, triangular-shaped whirls can be spotted near the enclosure's right wall. Denser isotherms exist between the cylinder and the right wall. It is reasonable to assume that greater heat is transported to the right wall.

As the overall heat transfer on the enclosure was analogous in cases of right and left location of cylinders. In order to avoid the recurrence of results, only the outcomes of the right location case are presented in the study. As permeability increases to $Da = 10^{-2}$, the recirculation zone on the right side of the cylinder expands, and the core of the inner eddy shifts towards the bottom wall. In the enclosure's left upper and lower portions, triangular shaped vortices are detected. In the region between the cylinder and the left wall, the isotherms, as seen in Fig. 5j–l, are denser. As a result, the left wall's heat dissipation rate is higher, and its Nusselt number is higher.

In Fig. 5m–r the cylinder is placed in top-diagonal and bottom-diagonal position. The region for recirculation increases as the cylinders are placed at corners of the enclosure. Small recirculating eddies are formed at corners. In Fig. 6r, the corner eddy diminishes as more amount of fluid enters the cylinder due to increased convective forces and permeability. The vortex near the bottom wall grows in size and begins to shift slightly higher.

The smaller inner eddy in the lower enclosure zone diminishes when the Rayleigh number is increased to 10^5 (Fig. 6). At $Da = 10^{-4}$, the fluid velocity increases, and the fluid penetrates the cylinder. As more fluid enters the cylinder, the recirculating region expands, and the core of the inner vortex shifts downwards at $Da = 10^{-2}$. At the same value of Da, the vortices shift upwards as the cylinder is moved towards top. The inner vortex eye slides downwards when the cylinder is pushed towards the bottom wall.

The recirculating whirl in the right section of the enclosure separates into two smaller vortices above and below the cylinder as the cylinder is moved from the centre to the right (Fig. 6j–l). As the amount of fluid entering the cylinder increases at Darcy number 10^{-2}, these vortices join a gigantic vortex travelling around and through the cylinder. In the left region, the focal point of recirculating eddies shifts downward and appears to lean towards the cylinder. This effect can also be observed in isothermal contours, as the isotherms progress toward the enclosure's left wall indicating convective effects on the opposite wall.

The abrupt expansion of the recirculation region whenever the cylinder is moved towards the top-diagonal and bottom-diagonal causes large-sized vortices. In case of top-diagonal location, the innermost vortex tends to move towards the cylinder and downwards when $Da = 10^{-2}$. In Fig. 6o, the number of the small recirculating eddies near the right wall increases.

The streamlines for the case of the cylinder placed in the bottom-diagonal position are shown in Fig. 6p–r. When the cylinder is pushed from the centre to the bottom-diagonal, a massive vortex in the enclosure's left zone splits into two smaller swirls above and the other lower vortex squeezes in the corner. Triangular-shaped vortices form as the Darcy number rises to 10^{-2}, and fluid recirculates around and through the cylinder. In the right section, the eye of recycling vortices turns downward. The thermal contours advance towards the corner opposite of the cylinder.

Figure 7 shows the streamlines at $Ra = 10^6$. The inner vortex elongates and moves upwards when $Ra = 10^6$, showing the flow of hot fluid towards the enclosure walls. Due to considerable convection effects, the symmetry along the horizontal centre line deteriorates. With larger convective effects, fluid velocity increases, and isothermal lines become more twisted. The amount of fluid entering the cylinder is less at $Ra = 10^4$ than at $Ra = 10^6$ for the same Darcy number (i.e. $Da = 10^{-4}$). The inner vortex tends to point downwards when the Darcy number rises from 10^{-6} to 10^{-4}. Two additional vortices form at the enclosure's bottom wall.

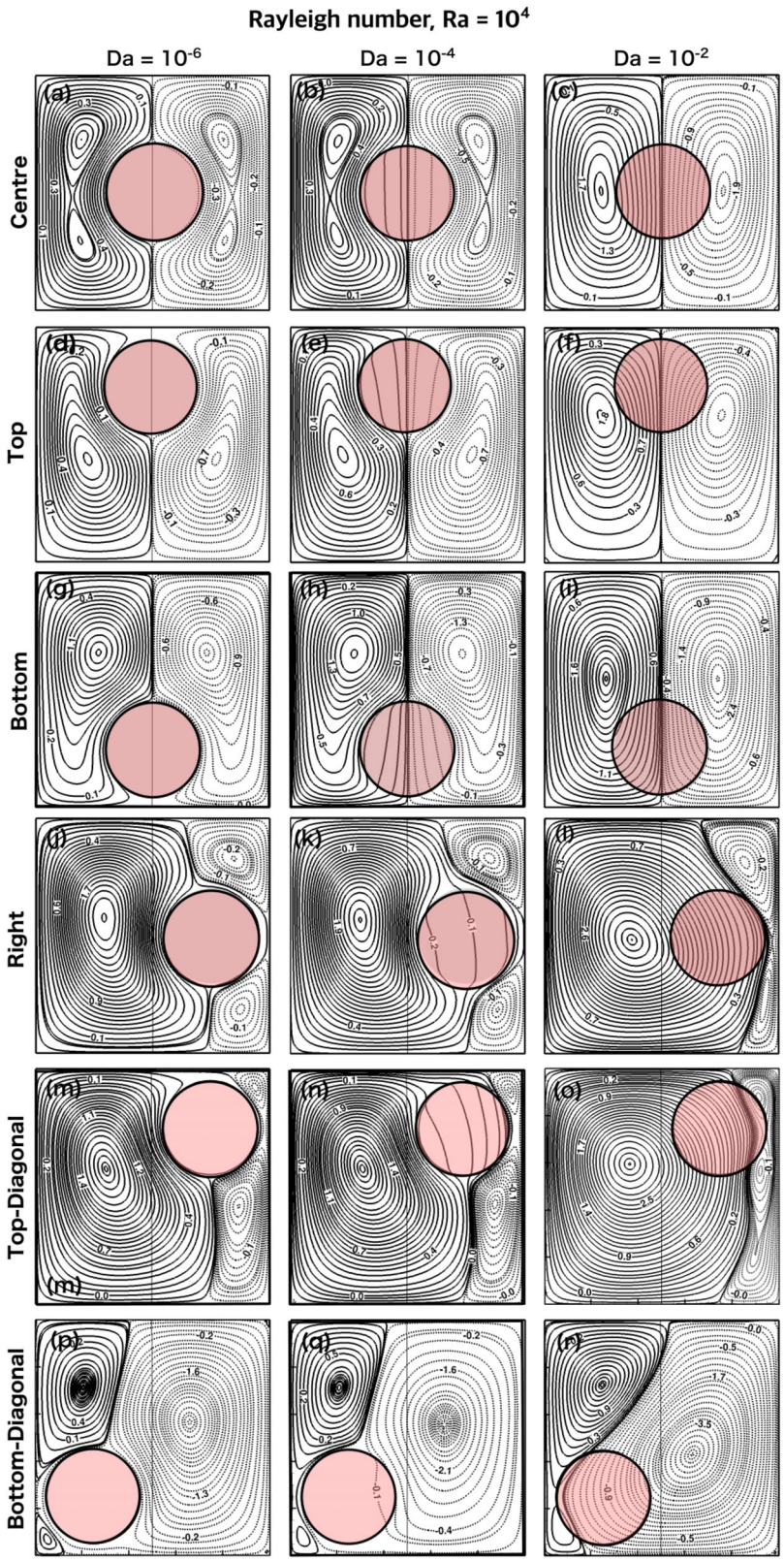

Fig. 5 Streamline contours in and around the porous circular cylinder placed at (**a**–**c**) centre, (**d**–**f**) top, (**g**–**i**) bottom, (**j**–**l**) right, and (**m**–**o**) top-diagonal and (**p**–**r**) bottom -diagonal in a cooled enclosure for different Darcy numbers (10^{-6}, 10^{-4} and 10^{-2}) at Rayleigh number $Ra = 10^4$

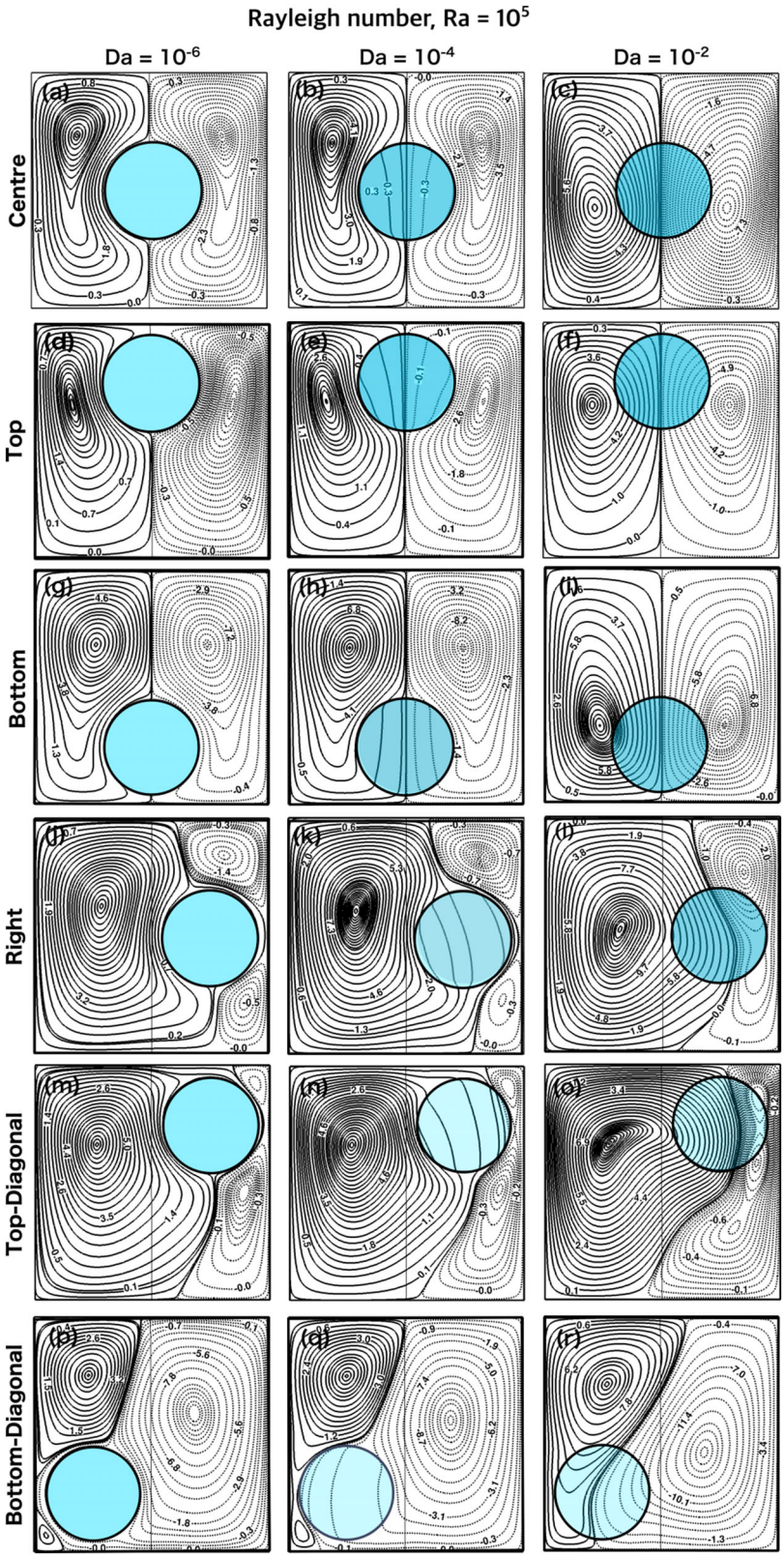

Fig. 6 Streamline contours in and around the porous circular cylinder placed at (**a**–**c**) centre, (**d**–**f**) top, (**g**–**i**) bottom, (**j**–**l**) right, and (**m**–**o**) top-diagonal and (**p**–**r**) bottom-diagonal in a cooled enclosure for different Darcy numbers (10^{-6}, 10^{-4} and 10^{-2}) at Rayleigh number $Ra = 10^5$

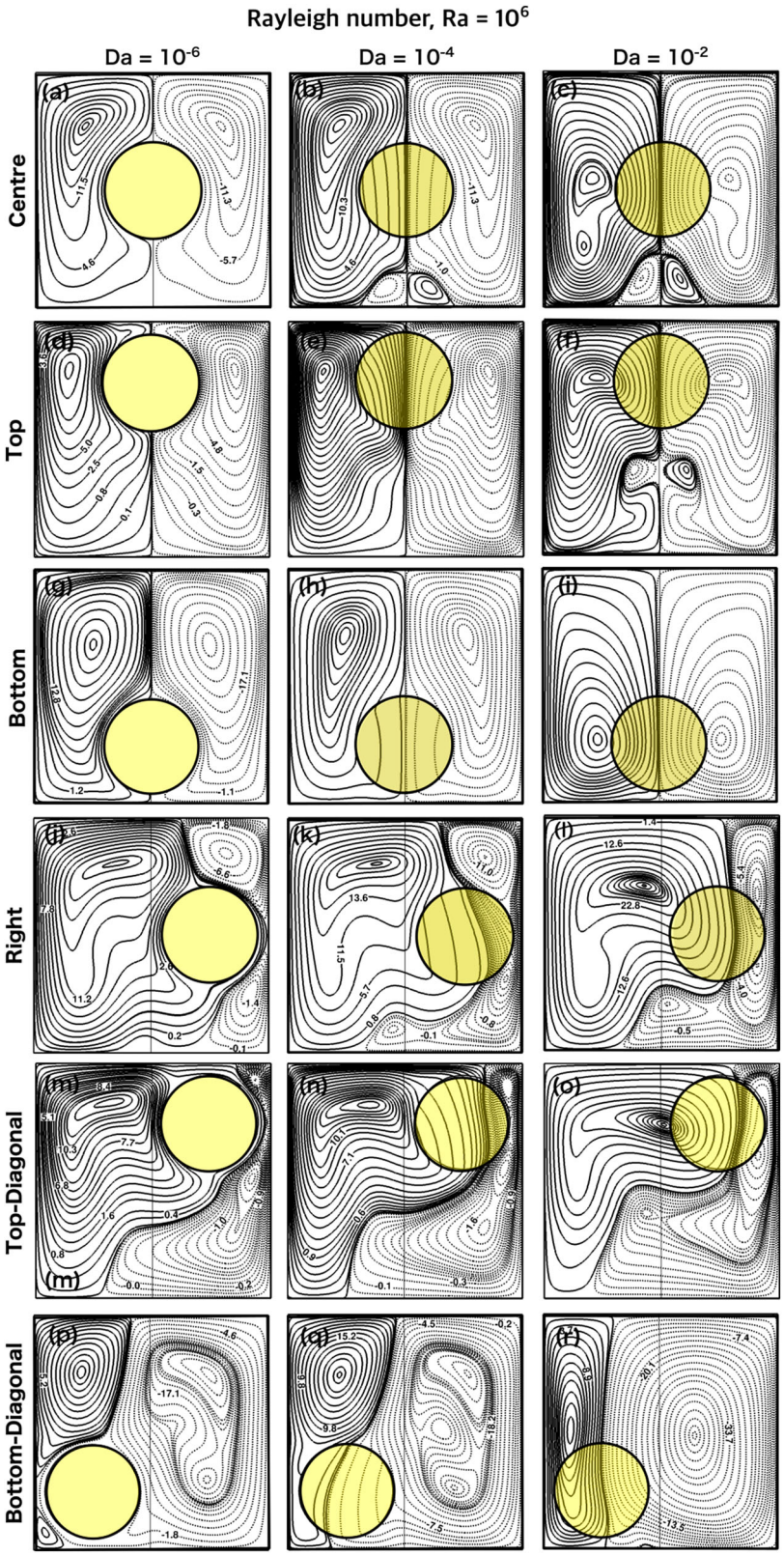

Fig. 7 Streamline contours in and around the porous circular cylinder placed at (**a**–**c**) centre, (**d**–**f**) top, (**g**–**i**) bottom, (**j**–**l**) right, and (**m**–**o**) top-diagonal and (**p**–**r**) bottom-diagonal in a cooled enclosure for different Darcy numbers (10^{-6}, 10^{-4} and 10^{-2}) at Rayleigh number $Ra = 10^6$

The size of these vortices grows as the Darcy number is increased to 10^{-2}. Less dense fluid is travelling away from gravity, as indicated by the plumes going towards the top wall, as shown in Fig. 10. Thinner boundary layers are detected as the permeability increases with the Darcy number. The streamlines move upwards as the cylinder is shifted towards the top. Two more minor eddies are spotted below the cylinder at $Da = 10^{-2}$. This is owing to the high velocity of enormous amounts of fluid moving through it. The isotherms illustrate that when the Darcy number rises, the thermal boundary layer beneath the cylinder grows thinner. The region between the top wall and the cylinder has more dense isotherms. Small vortices at the bottom wall are suppressed when the cylinder is pushed lower, and the size of the inner eddy above the cylinder grows. When the Darcy number is increased, the smaller eddies get smaller. The inner eddy shifts toward the bottom wall when $Da = 10^{-2}$. Massive upwelling isothermal contours occur, indicating greater convective effects. As the Darcy number is increased to 10^{-2}, the thickness of isotherms underneath the cylinder decreases.

In the right region, the core of recirculating eddies leans toward the cylinder. The thermal plumes migrate toward the enclosure's right side. The recirculating eddies in the left section of the enclosure divide into two smaller eddies above and underneath the cylinder as the cylinder is moved from the centre to the right (see Fig. 7j–l), forming a small vortex close to the bottom wall. These vortices converge to form a huge vortex that goes around and through the cylinder as the Darcy number is increased. There is an increase in the magnitude of the vortex near the bottom wall. As seen in Fig. 7j–l, the centre of recirculating eddies in the left region tends to lean toward the cylinder, and isotherms progress toward the enclosure's left region.

The cylinder placed in a diagonal position has dense isotherms near the surface, lying at the corner of the enclosure. On the opposite side, coarse isotherms are observed. In Fig. 7m–r, the creation of bigger vortices is aided by an increased area in the centre region of the enclosure as the cylinder is displaced diagonally. The instance of the cylinder in the top-diagonal (Fig. 7m–o) and bottom-diagonal is shown in Fig. 7p–r. A huge vortex in the left section of the enclosure with a minor vortex inclining towards the cylinder. The smaller vortices develop at the corner with additional vortices when $Da = 10^{-2}$ (Fig. 7o). In bottom-diagonal position, these vortices above the cylinder and at the corner of enclosure, unite to produce a single inner vortex that passes through and around the cylinder as the Darcy number increases.

In all cylinder positions, a thin boundary layer forms on one side of the cylinder, while the boundary layer on the other side is thicker, indicating heated fluid travels from the hot cylinder to the cold wall, showing an overall increase in natural convective effects. As a result, when the cylinder advances towards the bottom wall and bottom-diagonal, more significant heat transfer is obtained for all Rayleigh numbers.

The shape of isotherms over the cylinder in top-diagonal position changes from circular to pointing towards the right wall as Darcy number increases. As the Rayleigh number increases from 10^4 to 10^6, the thermal contours spread more towards the enclosure wall indicating heat transfer towards the cooled wall. On the other hand in case of bottom-diagonal position, the thermal plumes are denser in corners and tilted towards the top-right corner. This can also be certified by higher local Nusselt numbers along the bottom and left wall (see Fig. 3a–f). As the isotherms tend to move towards the top-right corner of enclosure, due to stronger thermal gradient, it enhances the heat transmission towards the opposite walls as well.

5 Conclusions

To compute flow and heat transfer through an isothermally heated porous circular cylinder in a cooled enclosure, the lattice Boltzmann method is utilised. The Darcy–Forchheimer model is used to model the porous medium. A force term is added to the BGK collision operator to account for the effects of inertial and viscous forces on the porous material. The effects of Rayleigh numbers (10^4 to 10^6) and Darcy numbers (10^{-6} to 10^{-2}) are explored on natural convection heat transfer. The impact of inserting a porous cylinder in the enclosure's centre, right, top, bottom, top-diagonal, and bottom-diagonal is studied. Using streamline distributions, isotherms, and the Nusselt number, the impact of the heated porous inner cylinder location on flow and heat transfer in the cooled enclosure is explored in depth. The following are the primary findings of the study:

- For all factors tested, the cylinder placement has a considerable impact on the flow and heat transport from the porous cylinder.
- When the cylinder is displaced vertically, the flow and heat fields settle into a symmetrical configuration around the enclosure's vertical centreline. As a result, there is twofold symmetry. The amount of fluid penetrating within the cylinder increases as the permeability increases. A larger boundary layer on the upper surface results in a bigger thermal gradient near the cylinder's bottom surface.

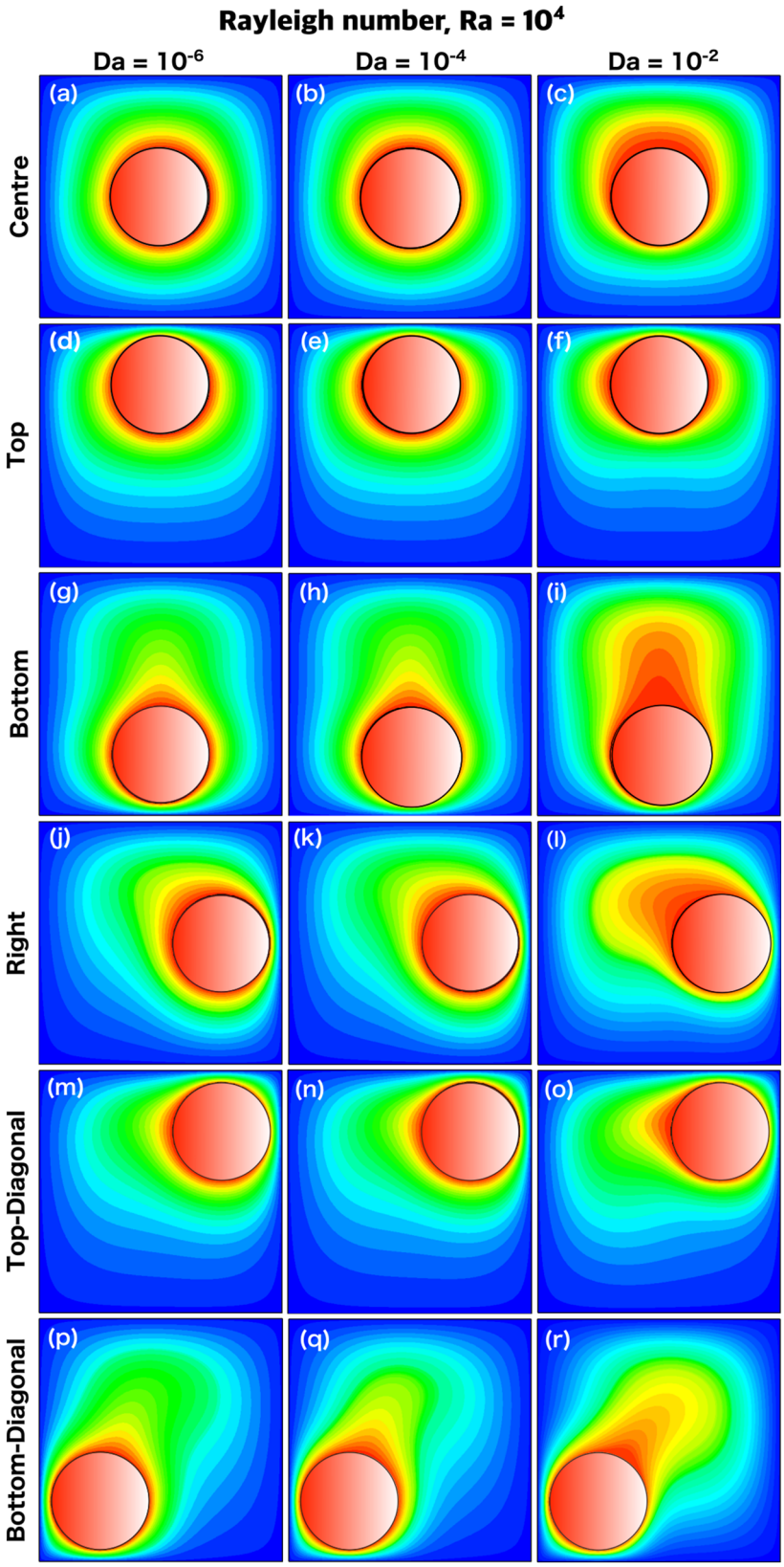

Fig. 8 Isotherms around the porous circular cylinder placed at (**a–c**) centre, (**d–f**) top, (**g–i**) bottom, (**j–l**) right, and (**m–o**) top-diagonal and (**p–r**) bottom-diagonal in a cooled enclosure for different Darcy numbers (10^{-6}, 10^{-4} and 10^{-2}) at $Ra = 10^4$

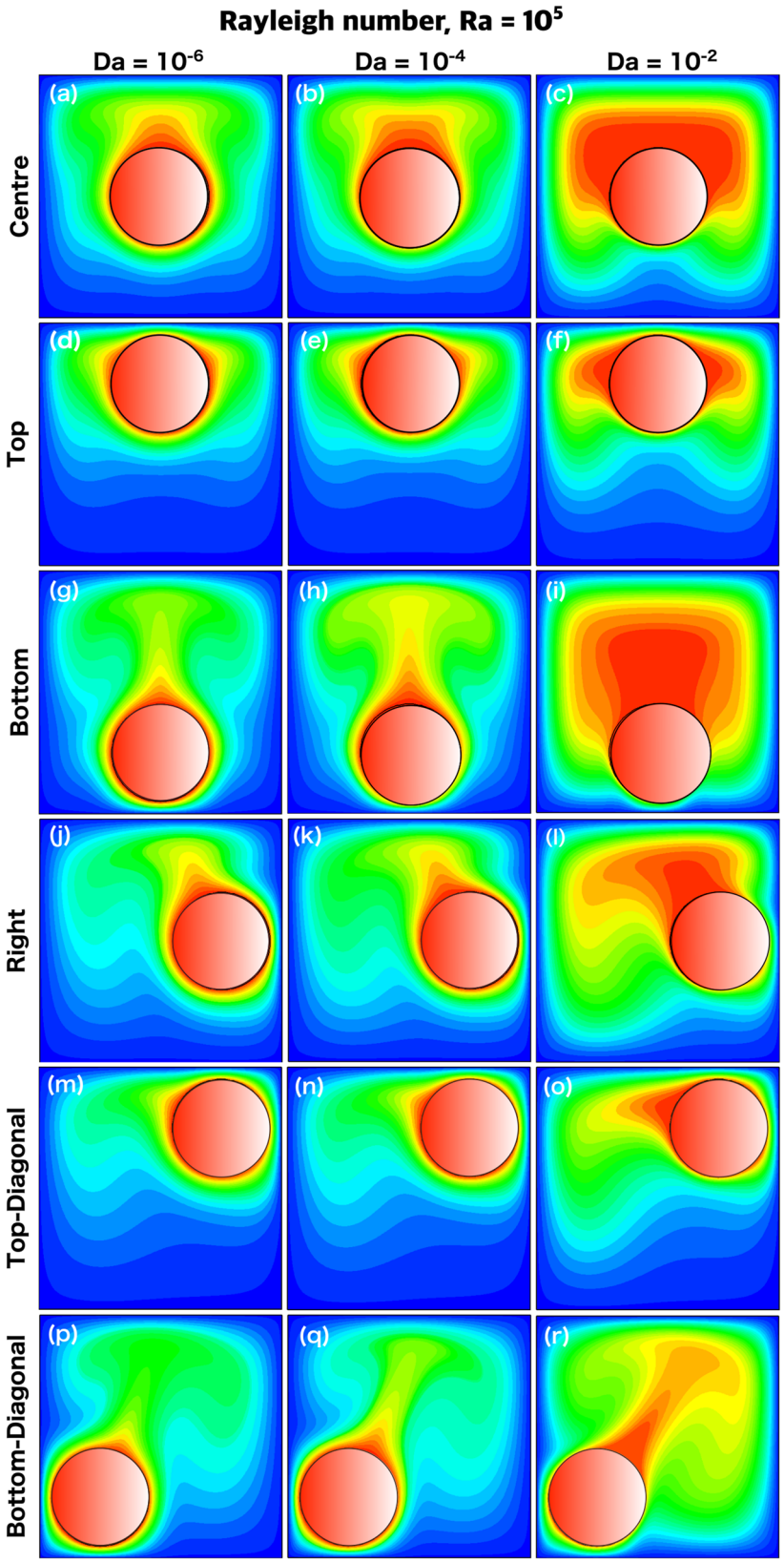

Fig. 9 Isotherms around the porous circular cylinder placed at (**a–c**) centre, (**d–f**) top, (**g–i**) bottom, (**j–l**) right, and (**m–o**) top-diagonal and (**p–r**) bottom-diagonal in a cooled enclosure for different Darcy numbers (10^{-6}, 10^{-4} and 10^{-2}) at $Ra = 10^5$

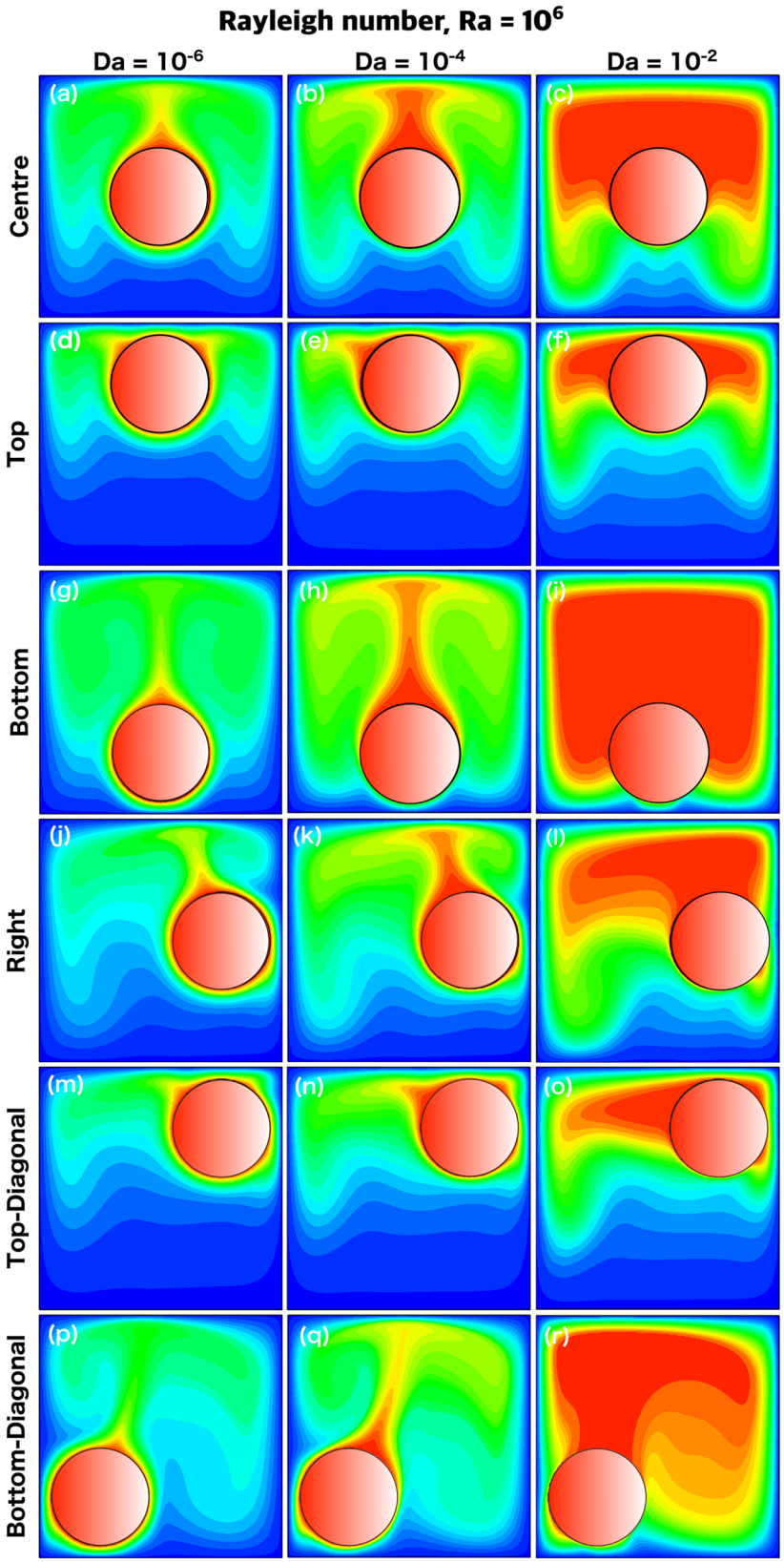

Fig. 10 Isotherms around the porous circular cylinder placed at (**a**–**c**) centre, (**d**–**f**) top, (**g**–**i**) bottom, (**j**–**l**) right, and (**m**–**o**) top-diagonal and (**p**–**r**) bottom-diagonal in a cooled enclosure for different Darcy numbers (10^{-6}, 10^{-4} and 10^{-2}) at $Ra = 10^6$

- For all Rayleigh numbers evaluated in this work, we find that the conductive effects are stronger at $Ra = 10^4$. Furthermore, bicellular vortices combine into a unicellular vortex at all points of the cylinder for Rayleigh numbers 10^5 and 10^6. At Rayleigh number 10^6, a significant amount of fluid travels through the permeable cylinder because convection effects are more pronounced.
- At all Darcy numbers, minimal amount of fluid penetrates inside the cylinder at $Da = 10^{-6}$. When the permeability is increased to 10^{-4}, a small amount of fluid enters the cylinder for a short time. Further increasing the Darcy number to 10^{-2} facilitates fluid movement and thereby improves heat dissipation.
- The centre position of the cylinder in the enclosure has a minimum rate of heat transfer in comparison with other cases for $Ra = 10^4$ and 10^5 as recirculation with bicellular vortices occurs around the cylinder. When $Ra = 10^4$, the mean Nusselt number rises by around 105% when the cylinder is moved from the centre to the bottom-diagonal at $Da = 10^{-2}$. The bottom-diagonal location has a higher heat dissipation rate for all Darcy and Rayleigh numbers.
- For all the cases studied, due to greater convective forces at the Rayleigh number 10^6, upwelling thermal plumes are obtained. When $Ra = 10^6$, the cylinder on the bottom-diagonal position has a 33% higher rate of heat transfer at $Da = 10^{-2}$ than the cylinder in the middle. The heat transfer rate is improved by slightly shifting the cylinder along the diagonal towards the bottom. Heat transfer is improved when the cylinder is placed close to the corners of the enclosure near the bottom wall. Hence, the bottom-diagonal configuration with Rayleigh number 10^6 and Darcy number 10^{-2} is best for obtaining a higher rate of heat dissipation.

Acknowledgements One of the authors (S.D) acknowledges the funds received from the Science and Engineering Research Board (SERB), a statutory body of Department of Science & Technology (DST), Government of India, through a Project Grant (File no. MTR/2019/001440).

Declarations

Data availability We confirm that the results file will be made available to readers upon request. Please contact the corresponding authors if you require the data.

References

1. Dhinakaran, S., Ponmozhi, J.: Heat transfer from a permeable square cylinder to a flowing fluid. Energy Convers. Manag. **52**(5), 2170–2182 (2011). https://doi.org/10.1016/j.enconman.2010.12.027
2. House, J.M., Beckermann, C., Smith, T.F.: Effect of a centred conducting body on natural convection heat transfer in an enclosure. Numer. Heat Transf. **18**(2), 213–225 (1990). https://doi.org/10.1080/10407789008944791
3. Alsabery, A.I., Sheremet, M.A., Chamkha, A.J., Hashim, I.: Conjugate natural convection of Al2O3–water nanofluid in a square cavity with a concentric solid insert using Buongiorno's two-phase model. Int. J. Mech. Sci. **136**, 200–219 (2018). https://doi.org/10.1016/j.ijmecsci.2017.12.025
4. Moukalled, F., Acharya, S.: Natural convection in the annulus between concentric horizontal circular and square cylinders. J. Thermophys. Heat Transf. **10**(3), 524–531 (1996). https://doi.org/10.2514/3.820
5. Roychowdhury, D.G., Das, S.K., Sundararajan, T.: Numerical simulation of natural convective heat transfer and fluid flow around a heated cylinder inside an enclosure. Heat Mass Transf. **38**(7), 565–576 (2002). https://doi.org/10.1007/s002310100210
6. Nabavizadeh, S.A., Talebi, S., Sefid, M., Nourmohammadzadeh, M.: Natural convection in a square cavity containing a sinusoidal cylinder. Int. J. Therm. Sci. **51**, 112–120 (2012). https://doi.org/10.1016/j.ijthermalsci.2011.08.021
7. Jami, M., Mezrhab, A., Bouzidi, M., Lallemand, P.: Lattice Boltzmann method applied to the laminar natural convection in an enclosure with a heat-generating cylinder conducting body. Int. J. Therm. Sci. **46**(1), 38–47 (2007). https://doi.org/10.1016/j.ijthermalsci.2006.03.010
8. Jami, M., Mezrhab, A., Naji, H.: Numerical study of natural convection in a square cavity containing a cylinder using the lattice Boltzmann method. Eng. Comput. (2008). https://doi.org/10.1108/02644400810881400
9. Kim, B.S., Lee, D.S., Ha, M.Y., Yoon, H.S.: A numerical study of natural convection in a square enclosure with a circular cylinder at different vertical locations. Int. J. Heat Mass Transf. **51**(7–8), 1888–1906 (2008). https://doi.org/10.1016/j.ijheatmasstransfer.2007.06.033
10. Hussain, S.H., Hussein, A.K.: Numerical investigation of natural convection phenomena in a uniformly heated circular cylinder immersed in square enclosure filled with air at different vertical locations. Int. Commun. Heat Mass Transf. **37**(8), 1115–1126 (2010). https://doi.org/10.1016/j.icheatmasstransfer.2010.05.016
11. Yoon, H.S., Ha, M.Y., Kim, B.S., Yu, D.H.: Effect of the position of a circular cylinder in a square enclosure on natural convection at Rayleigh number of 10^7. Phys. Fluids **21**(4), 047101 (2009). https://doi.org/10.1063/1.3112735

12. Kang, D.H., Ha, M.Y., Yoon, H.S., Choi, C.: Bifurcation to unsteady natural convection in square enclosure with a circular cylinder at Rayleigh number of 10^7. Int. J. Heat Mass Transf. **64**, 926–944 (2013). https://doi.org/10.1016/j.ijheatmasstransfer.2013.05.002
13. Nithiarasu, P., Seetharamu, K.N., Sundararajan, T.: Natural convective heat transfer in a fluid saturated variable porosity medium. Int. J. Heat Mass Transf. **40**(16), 3955–3967 (1997). https://doi.org/10.1016/S0017-9310(97)00008-2
14. Vijaybabu, T.R.: Influence of permeable circular body and CuO–H_2O nanofluid on buoyancy-driven flow and entropy generation. Int. J. Mech. Sci. **166**, 105240 (2020). https://doi.org/10.1016/j.ijmecsci.2019.105240
15. Hu, J.T., Mei, S.J.: Combined thermal and moisture convection and entropy generation in an inclined rectangular enclosure partially saturated with porous wall: nonlinear effects with Soret and Dufour numbers. Int. J. Mech. Sci. **199**, 106412 (2021). https://doi.org/10.1016/j.ijmecsci.2021.106412
16. Lauriat, G., Prasad, V.: Non-Darcian effects on natural convection in a vertical porous enclosure. Int. J. Heat Mass Transf. **32**, 2135–2148 (1989). https://doi.org/10.1016/0017-9310(89)90120-8
17. Chen, X.B., Yu, P., Winoto, S.H., Low, H.T.: Free convection in a porous wavy cavity based on the Darcy–Brinkman–Forchheimer extended model. Numer. Heat Transf. Part A **52**, 377–397 (2007). https://doi.org/10.1080/10407780701301595
18. Kumari, M., Nath, G.: Unsteady natural convection from a horizontal annulus filled with a porous medium. Int. J. Heat Mass Transf. **51**, 5001–5007 (2008). https://doi.org/10.1016/j.ijheatmasstransfer.2008.01.030
19. Mohamad, A.A.: Lattice Boltzmann Method: Fundamentals and Engineering Applications with Computer Codes. Springer, London (2011). https://doi.org/10.1007/978-1-4471-7423-3
20. Lahmer, E.B., Admi, Y., Moussaoui, M.A., Mezrhab, A.: Improvement of the heat transfer quality by air cooling of three-heated obstacles in a horizontal channel using the lattice Boltzmann method. Heat Transf. (2022). https://doi.org/10.1002/htj.22481
21. Guo, Z., Zhao, T.S.: Lattice Boltzmann model for incompressible flows through porous media. Phys. Rev. E **66**(3), 036304 (2002). https://doi.org/10.1103/PhysRevE.66.036304
22. Kozeny, J.: Ueber kapillare Leitung des Wassers im Boden. Sitzungsber Akad. Wiss., Wien, Royal Academy of Science, Vienna, Proc. Class I 136(2a): 271–306 (1927)
23. Carman, P.C.: Fluid flow through granular beds. Trans. Inst. Chem. Eng. **15**, 150–166 (1937)
24. Carman, P.C.: Flow of Gases Through Porous Media. Butterworths Scientific Publications, New York (1956)